Journal of Inorganic and Organometallic Polymers and Materials (2018) 28:2427–2438
https://doi.org/10.1007/s10904-018-0930-8

Hydrogenation of *p*-Nitrobenzoic Acid by Gold and Palladium Nanoparticles Immobilized Within Macroporous Amphoteric Cryogels in Aqueous Solution

Sarkyt Kudaibergenov[1,2] · Moldir Dauletbekova[1,2] · Gaukhar Toleutay[1] · Sana Kabdrakhmanova[1,2] · Tulegen Seilkhanov[3] · Khabib Abdullin[4]

Received: 18 April 2018 / Accepted: 21 July 2018 / Published online: 24 July 2018

Abstract
Aqueous solutions of sodium salt of *p*-nitrobenzoic acid (*p*-NBA) were hydrogenated in mild conditions in the presence of palladium (PdNPs) and gold nanoparticles (AuNPs) immobilized within macroporous amphoteric cryogel based on *N,N*-dimethylaminoethylmethacrylate (DMAEM) and methacrylic acid (MAA). The morphology of the macroporous catalyst DMAEM-*co*-MAA/AuNPs was characterized using SEM. The pore sizes of sponge-like porous structure of cryogels are in the range of 5–40 μm, while the average sizes of AuNPs immobilized within the macroporous amphoteric cryogel are 80 ± 20 nm. The reduction of *p*-NBA to *p*-aminobenzoic acid (*p*-ABA) and further to by-products *p,p′*-azodibenzoate and sodium 4-(4-aminobenzamido)benzoate was confirmed by Raman and ^{1}H NMR spectroscopy. The conversion degree, kinetic parameters, and activation energies of hydrogenation of *p*-NBA were found.

Keywords Macroporous amphoteric cryogel · Palladium and gold nanoparticles · Hydrogenation · *p*-Nitrobenzoic acid · Macroporous flow-through catalytic reactor

1 Introduction

Functional polymers and their metal complexes including metal nanoparticles supported on the surface and/or inside of the polymer matrix play a crucial role in catalysis [1–3]. A new approach to the synthesis of immobilized catalysts of the mixed type, in particular, frontal polymerization of metal-containing monomers in the presence of a highly dispersed inorganic support was developed by other authors [4]. The polymer-immobilized PdNPs on the SiO_2 have proved to be an efficient catalyst for the reduction of nitrotoluene derivatives. Immobilization of metal nanoparticles using macroporous gels will open new perspectives for development of effective catalytic systems for various chemical reactions [5, 6]. Cryogels typically have interconnected macropores (or supermacropores), allowing unhindered diffusion of solutes of practically any size, as well as mass transport of nano- and even microparticles [7–9]. Therefore alongside the well-known utilization of cryogels in medicine, biotechnology and biology, they could also be used in catalysis [10, 11]. The main advantage of cryogels in catalysis is their macroporous structure, which can provide both loading of metal nanoparticles and unhindered liquid flux within cryogels. Superporous cryogels of poly(2-hydroxy ethyl methacrylate) and poly(3-sulfopropyl methacrylate) [12], poly(acrylic acid) [13], poly(4-vinylpyridine) [14], poly(2-acrylamido-2-methyl-1-propansulfonic acid) [15], poly[2-(methacryloyloxy)ethyl]dimethyl(3-sulfopropyl) ammoniumhydroxide [16] and its templated metal nanoparticle composites (Co, Ni, Cu, and Fe) were used in the

✉ Sarkyt Kudaibergenov
skudai@mail.ru

Tulegen Seilkhanov
tseilkhanov@mail.ru

Khabib Abdullin
kh.a.abdullin@mail.ru

1 Laboratory of Engineering Profile, K.I. Satpayev Kazakh National Research Technical University, Almaty, Kazakhstan

2 Institute of Polymer Materials and Technology, Almaty, Kazakhstan

3 Sh. Ualikhanov Kokshetau State University, Abay Str. 76, 020000 Kokshetau, Kazakhstan

4 National Nanotechnological Laboratory, Al-Farabi Kazakh National University, Almaty, Kazakhstan

redox reaction of $NaBH_4$ and hydrogenation of nitro compounds, such as 4-nitrophenol (4-NP), 2-nitrophenol (2-NP) and 4-nitroaniline (4-NA).

The catalytic reduction of *p*-nitrobenzoic acid (*p*-NBA) to *p*-aminobenzoic acid (*p*-ABA) has been performed in the presence of Pt/C and Pd/C [17–19], resin-bound Pd and Ag nanocomposites, Ag/Au nanoparticles supported on a commercially available anion exchange resin by LbL technique [20], colloidal Ag nanoparticles [21–23], *cis*-[Rh(CO)(2)(amine)(2)](PF6) [24], and electrochemically [25]. The derivatives of *p*-ABA are widely used as anesthetics such as novocaine, butamben, procaine, risocaine, and as ingredient in sunscreen formulations [25, 26]. The method of obtaining of *p*-ABA has been patented [27]. Recently, magnetically recoverable gold nanorods [28] and palladium nanoparticles supported on Fe_3O_4@C [29], polybenzimidazole supported rhodium [29, 30], hollow aluminosilicate microsphere [31] and magnetic graphene oxide [32] have been applied in the selective reduction of nitroarenes into corresponding aminoarenes. Usually in industry, the catalytic reduction of nitro compounds by hydrogen is carried out at a relative high pressure (10–50 bar) and temperature (100–150 °C), which requires the use of a special and safe catalytic reactor [33].

Earlier [34–37], we studied the complexation of macroporous cryogels based on DMAEM-co-MAA with dyes, surfactants and proteins, and evaluated their catalytic activity with respect to reduction of 4-NP. The kinetic parameters TON, TOF, and activation energy of hydrogenation of 4-NP have been calculated.

In the present communication we suggest a basic catalytic reduction of *p*-NBA by PdNPs and AuNPs supported on a cryogel matrix of DMAEM-*co*-MAA. The main reason for selecting amphoteric cryogels as a medium is that the acid-base groups of a polymeric matrix easily reduce the gold ions and retain the substrate molecules via hydrogen bonds or electrostatic interactions on the surface of cryogels to prolong their longevity, thus promoting the catalytic conversion. Another advantage of our approach is that aqueous solutions of *p*-NBA passing through the macroporous heterogenic polymer matrix are converted to a final product—*p*-ABA and by-products, following the separation of the key product from the catalyst.

2 Experimental Part

2.1 Materials

Macroporous amphoteric cryogel DMAEM-*co*-MAA of equimolar composition crosslinked by 2.5 mol% *N,N*-methylenebisacrylamide was used for the flow-through catalytic experiments [36, 37]. Standard aqueous solutions of tetrachlorauric acid $HAuCl_4$ and tetrachloropalladate acid H_2PdCl_4 with concentration 100 mg L^{-1}, *p*-nitrobenzoic acid (*p*-NBA), *p*-aminobenzoic acid (*p*-ABA), and sodium borohydride ($NaBH_4$) were purchased from Sigma-Aldrich.

2.2 Methods

FTIR and Raman spectra were registered on Carry 660 (Agilent, USA) and NTEGRA Spectra spectrometers (NT-MDT), using 473 nm excitation. Absorption spectra were recorded with UV–Vis spectrophotometer (Specord 210 plus BU, Germany) at room temperature. ^{1}H NMR spectra of *p*-NBA and *p*-ABA in D_2O were registered on an impulse Fourier NMR spectrometer Bruker 400 MHz (Bruker, Germany). Scanning electron microscopy (SEM) images were obtained on a high resolution SEM (Zeiss Merlin High-resolution SEM). SEM images were analyzed using open access software "ImageJ" to evaluate the size distribution of AuNPs.

2.3 Immobilization of PdNPs and AuNPs Within the Macropores of DMAEM-*co*-MAA Cryogel

Immobilization of PdNPs and AuNPs within DMAEM-*co*-MAA cryogel matrix was carried out as follows. Dry cryogel (22.5 mg) was immersed to 18 mL of deionized water containing 2 mL $HAuCl_4$ (or H_2PdCl_4) with a concentration of 100 mg L^{-1}, and boiled. After 30 min of heating, the colorless DMAEM-*co*-MAA cryogel sample turned into a dark red (or black) color. The appearance of the maximum absorption at 530 nm confirms the stabilization of gold nanoparticles by DMAEM-*co*-MAA. The DMAEM-*co*-MAA cryogel containing PdNPs and AuNPs is further abbreviated as DMAEM-*co*-MAA/PdNPs and DMAEM-*co*-MAA/AuNPs.

2.4 Evaluation of the Catalytic Activity of DMAEM-*co*-MAA/PdNPs and DMAEM-*co*-MAA/AuNPs

Hydrogenation of *p*-NBA was carried out in a flow through catalytic reactor, represented in Fig. 1. The reactor consists of a glass tube with an inner diameter of 6–7 mm and a height of 100 mm, which is filled with dry cryogel pieces with a diameter of 5 mm and a height of 10 mm. The bottom part of the glass tube is closed by a Shott filter ending with a valve. At first, 10 or 15 mL of deionized water is passed through the cryogel sample. Due to quick swelling of cryogel, tight sealing between the inner wall of the glass tube and the swollen sample takes place.

In case of *p*-NBA hydrogenation, the concentration of *p*-NBA was kept constant and equal to 5×10^{-5} mol L^{-1} while the concentration of $NaBH_4$ varied from 1×10^{-2} to 2.5×10^{-3} mol L^{-1}. For example, a 10 mL aqueous solution composed of 1 mL 5×10^{-4} mol L^{-1} *p*-NBA, 1 mL

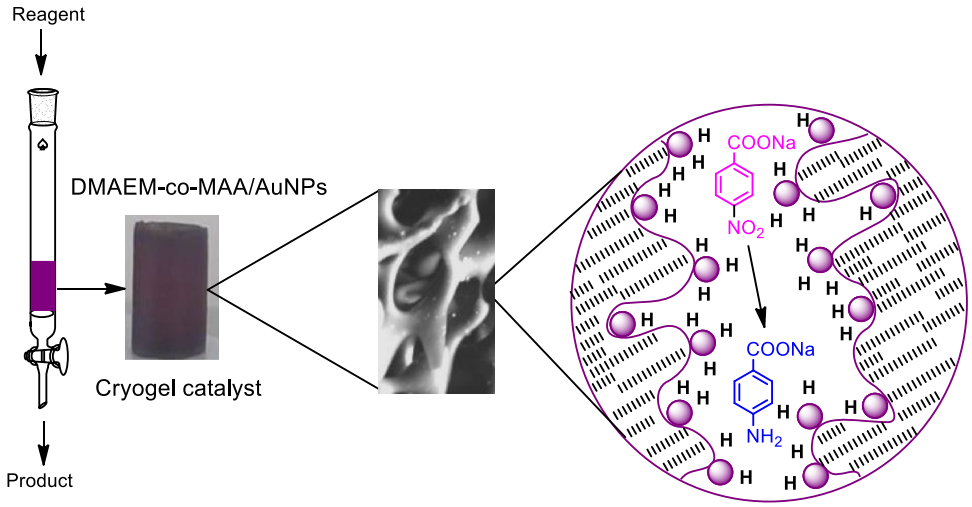

Fig. 1 Schematic representation of flow-through catalytic reactor for the catalytic reduction *p*-NBA by DMAEM-*co*-MAA/AuNPs catalyst

1×10^{-1} mol L^{-1} $NaBH_4$, and 8 mL of deionized water was pumped through the DMAEM-*co*-MAA cryogel sample containing AuNPs with the help of peristaltic pump (the flowing rate is 1.5 mL min^{-1}) [35]. Each experiment was repeated 4–5 times. Time dependent absorption spectra of substrate and product were recorded in the UV–Vis spectrophotometer over a scanning range from 200 to 450 nm every 15 s. The concentrations of *p*-ABA and *p*-NBA were determined from calibration graphs at 266 and 274 nm, respectively.

3 Results and Discussion

3.1 Morphology of DMAEM-*co*-MAA/AuNPs Macroporous Cryogel

For SEM experiments, the cryogel samples containing the gold nanoparticles were washed out by distilled water then successively washed out by 25, 50, 75 and 96% ethanol to dehydrate, then dried in air and finally in a vacuum oven to a constant mass at room temperature. According to SEM images, the average pore size of the DMAEM-*co*-MAA sample varied from 5 to 40 μm (Fig. 2). The gold nanoparticles are mostly located on the surface of macropore walls. SEM images were analyzed using open access software, ImageJ, to evaluate the size distribution of AuNPs. The findings showed that the average size of AuNPs is 80 ± 20 nm.

3.2 Catalytic Activity of DMAEM-*co*-MAA/AuNPs in Hydrogenation of *p*-NBA

Catalytic reduction of *p*-NBA to *p*-ABA over DMAEM-*co*-MAA/AuNPs catalyst proceeds via formation of intermediate compounds via the following Scheme 1 [18].

It should be noted that the mixture of *p*-NBA and $NaBH_4$ fluxed through the DMAEM-*co*-MAA cryogel does not produce *p*-ABA in the absence of immobilized AuNPs. In the presence of DMAEM-*co*-MAA/AuNPs, the

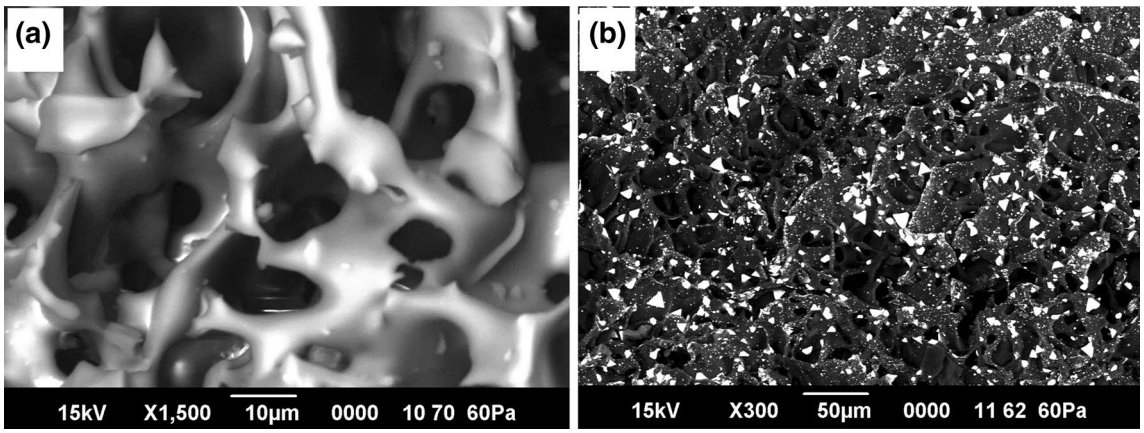

Fig. 2 Morphology of pristine (**a**) and AuNPs immobilized (**b**) macroporous amphoteric cryogels

absorption peak at 274 nm that belongs to *p*-NBA gradually increases and shifts to 264 nm, which is characteristic for the sodium salt of *p*-ABA [38] (Fig. 3a). Time dependent conversion of *p*-NBA to *p*-ABA was calculated from the 1st to 5th cycles. The average reduction degree of *p*-NBA over 18–21 min is 58%.

It should be noted that starting from the 6th cycle of *p*-NBA hydrogenation, an additional two absorption peaks at 285 and 311 nm are observed (Fig. 3b). The intensity of these peaks does not change up to the 12th cycle. It is supposed that the appearance of the two peaks is connected with formation of *p,p′*-azodibenzoate due to catalytic coupling condensation of nitroso compound with hydroxylamine, and with participation of hydrogen atoms that are generated from sodium borohydride through formation of azoxy compound, which is reduced in a series of consecutive steps to the azocompound (Scheme 2).

The formation of *p,p′*-azodibenzoate is confirmed by Raman spectroscopy (Fig. 4; Table 1).

Surface-enhanced Raman scattering (SERS) is an effective tool to detect, at trace levels, the reactants, products or by-products in reactions that take place on the surface of the metal nanoparticles [39]. The formation of azodibenzoate from *p*-NBA adsorbed on Ag island films or Ag nanoprticles was observed by SERS and evidenced by the appearance of a strong band near 1460 cm^{-1} and a strong doublet near 1150 cm^{-1} [40–42]. Later on, this finding was confirmed by other authors [42–44] using the SERS experiments. After hydrogenation of *p*-NBA, the Raman spectra contain mostly the characteristic bands of *p*-ABA. However, additional bands at 1133, 1149, 1447 cm^{-1} in powder and at 1133, 1153, 1451 cm^{-1} in aqueous solution appeared in hydrogenated product of *p*-NBA. They may belong to –N=N– groups of *p,p′*-azodibenzoate. Other authors [38, 39] compared the catalytic activity of mono- and bimetallic nanoparticles

Scheme 1 Hydrogenation of *p*-NBA over DMAEM-*co*-MAA/AuNPs catalyst

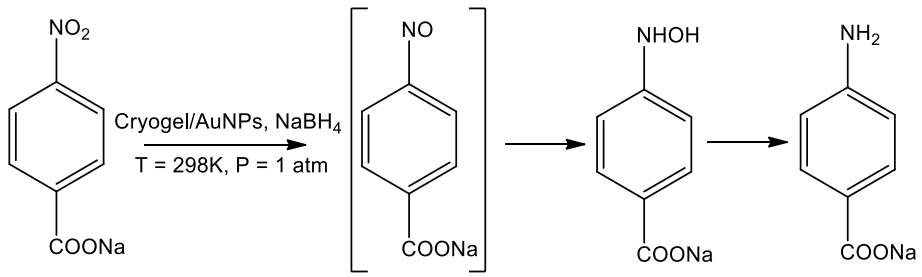

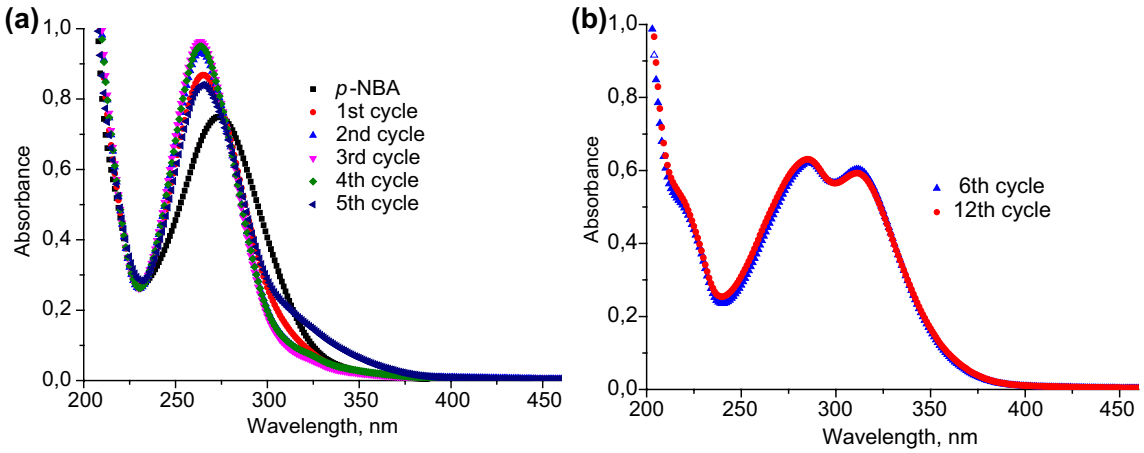

Fig. 3 **a** Absorption spectra of *p*-NBA hydrogenated from the 1st to 5th cycles. **b** Absorption spectra of *p*-NBA hydrogenated from the 6th to 12th cycles. Molar ratio of [*p*-NBA]:[$NaBH_4$] = 1:200. [*p*-NBA] = 5×10^{-5} mol L^{-1}. [$NaBH_4$] = 1×10^{-2} mol L^{-1}. T = 298 K

Scheme 2 Possible mechanism of formation of *p,p′*-azodibenzoate

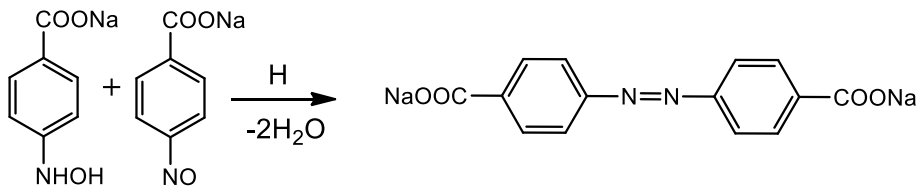

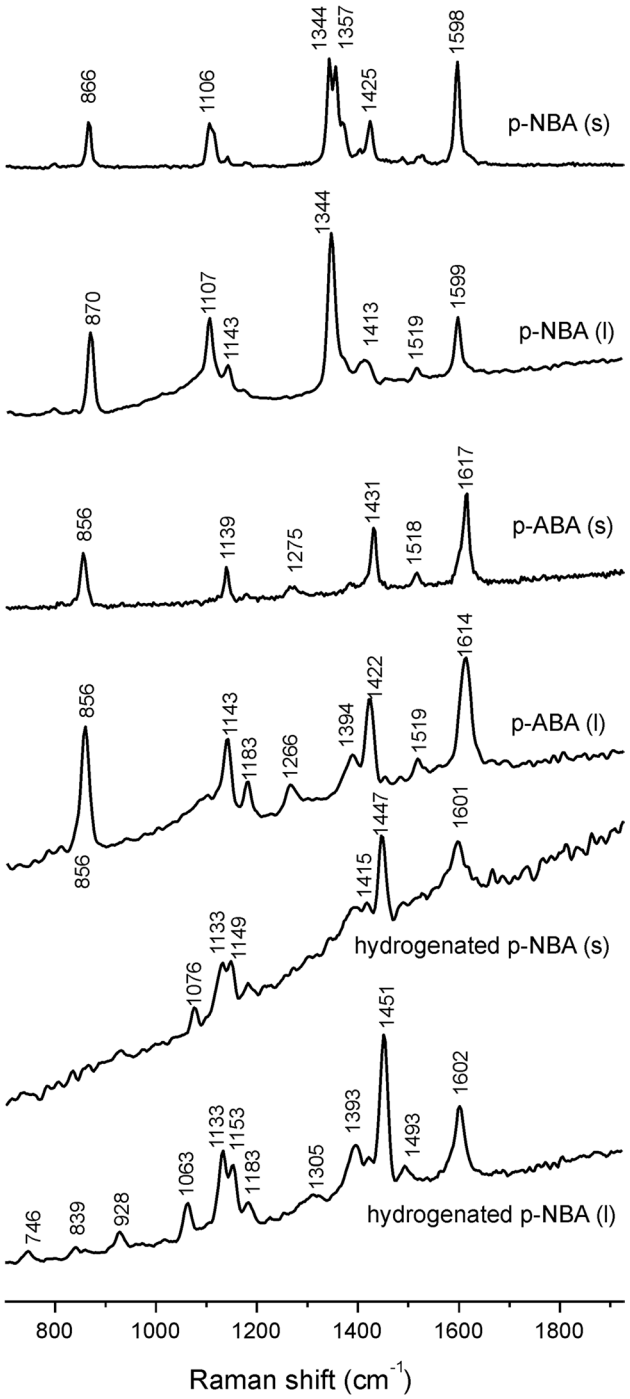

Fig. 4 Comparison of Raman spectra of *p*-NBA, *p*-ABA and hydrogenated product of *p*-NBA in solid state and aqueous solution (where **s** is solid, **l** is liquid)

composed of pure Ag and Ag/Pd (96:4 mol/mol) colloids and the SERS spectra of *p*-NBA. In pure Ag colloid, only bands attributable to the carboxylate anion of *p*-NBA are seen, while in Ag/Pd colloid after 1 day the SERS bands that belong to the *p,p′*-azodibenzoate anion are detected (Fig. 5).

Comparison of Raman spectrum of the hydrogenated product of *p*-NBA over DMAEM-*co*-MAA/AuNPs catalyst (as powder and aqueous solution) and SERS spectrum of *p*-NBA over Ag/Pd colloids (Fig. 5) shows that the characteristic bands of functional groups in both cases are the same and that they belong to *p,p′*-azodibenzoate. The only difference is the appearance of additional bands at 1063 and 1076 cm^{-1} in the Raman spectra of hydrogenated product of *p*-NBA over DMAEM-*co*-MAA/AuNPs catalyst. These bands can be can be assigned to *p*-ABA adsorbed on the surface of AuNPs [45]. Thus, intensive Raman bands at 1133, 1149, 1153, 1447 and 1451 cm^{-1} that exist in hydrogenated product of *p*-NBA can be used for identification of reaction products and prediction of reaction mechanisms.

The ^{1}H NMR spectra of *p*-NBA, *p*-ABA and hydrogenated product of *p*-NBA are compared in Fig. 6. The ^{1}H NMR spectra of *p*-ABA contain the doublets at δ = 6.65 and 7.55 ppm that belong to the $H^{2,6}$ and $H^{3,5}$ protons of the aromatic ring. However, NH_2 groups in *p*-ABA are not seen in ^{1}H NMR spectra due to easy replacement of amine protons by deuterium. The ^{1}H NMR spectra of *p*-NBA consist of doublets at δ = 7.75 and 7.87 ppm that belong to the $H^{2,6}$ and $H^{3,5}$ protons of the aromatic ring. In the hydrogenated product of *p*-NBA, together with doublets at δ = 6.65 and 7.55 ppm, a new intense signal appears at δ = 8.28 ppm, which may be related to NH groups of amide bonds formed due to condensation of terminal NH_2 and COONa groups of *p*-ABA (Scheme 3). According to [48], a peak around of δ = 8.31 ppm is attributed to NH groups.

Other authors [49] performed a direct condensation polymerization of N-alkylated *p*-ABA, containing methyl, propyl, butyl, pentyl, heptyl, octyl and heptadecyl substituents, in order to obtain N-alkylated poly(*p*-benzamide) using hexachloroethane, triphenylphosphine and pyridine as condensation reagents (Scheme 4).

Analysis of integral peaks of ^{1}H NMR spectra of *p*-NBA and *p*-ABA reveals that approximately 62.6% of *p*-NBA is converted to *p*-ABA (Fig. 7).

To confirm the condensation of *p*-ABA and formation of sodium 4-(4-aminobenzamido)benzoate, we have run an aqueous solution of pure *p*-ABA 10 times through DMAEM-*co*-MAA/AuNPs. As seen from ^{1}H NMR spectra, in addition to $H^{2,6}$ and $H^{3,5}$ protons of the aromatic ring, an intense signal at δ = 8.28 ppm, appears which is specific to NH groups (Fig. 8).

From the results of Fig. 8, the content of NH groups was calculated. It was found that the number of NH groups is 44.6%, meaning that an equal amount of *p*-ABA is converted to sodium 4-(4-aminobenzamido)benzoate.

The reduction rate kinetics are treated as a pseudo-first-order reaction with regards to *p*-NBA concentration. The absorbance A_t at time t divided by the absorbance A_0

Table 1 Raman spectra of *p*-NBA, *p*-ABA and hydrogenated products of *p*-NBA

p-NBA, cm^{-1}		*p*-ABA, cm^{-1}		Hydrogenated product of *p*-NBA, cm^{-1}		Band assignments[a] and Refs
Solid	Aqueous solution	Solid	Aqueous solution	Solid	Aqueous solution	
866 s	870 s					NO_2 bending [47]
		856 s	860 s		839 vw	COO^- bending [45, 46]
				1076 w	1063 m	Peaks can be assigned to *p*-ABA adsorbed on the surface of AuNPs [44]
1106 s	1107 s					C–NO_2 stretches coupled with C–H in-plane bending [47]
				1133 m	1133 s	Peaks can be assigned to *p,p′*-azodibenzoate [39]
1143 vw	1143 w	1139 m	1143 s			C–CO_2 stretches coupled with C–H in plane bending [47]
				1149 m	1153 m	Peaks can be assigned to *p,p′*-azodibenzoate [39, 40]
			1183 w		1183 w	C–N stretching coupled with C–H in-plane bending [47]
		1275 w	1266 w		1276 w	C–N stretching [45]
1344 vs	1344 vs					NO_2 symmetric stretching [47]
1357 vs						Symmetric stretches of the carboxylate groups [47]
			1394 w			COO^- symmetric stretching [42]
				1394 vw	1393 w	N=N stretching coupled with C–C stretching [47]
1425 s	1413 w	1431 s	1422 s			Can be ascribed to photo-induced reduction products of PNBA [40, 45]
				1447 vs	1451 vs	N=N stretching coupled with C–C stretching [41]
		1518 w	1519 w			In-plane benzene ring stretching vibrations [42]
1598 vs	1599 s					C–C sretching of benzene [47] or C–C stretching in two benzene rings [49]
				1601 s	1602 s	
		1617 vs	1614 s			NH_2 bending [42]

s strong, *m* medium, *w* weak, *vs* very strong, *vw* very weak

[a]Identification of Raman spectra is based on literature data [39–47]

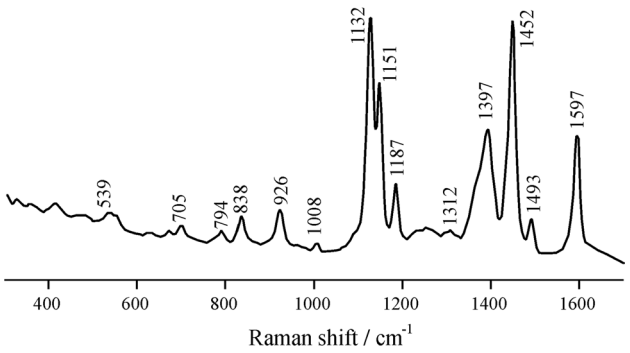

Fig. 5 SERS spectrum of *p*-NBA in the presence of Ag/Pd colloid obtained after 1 day. The excitement line is 514.5 nm. Reproduced with permission from Ref. [39]

measured at $t = 0$ gives the corresponding concentration ratios C/C_0 of *p*-NBA. Thus we have the following equation:

$$\frac{dC_t}{dt} = -k_{app}t \text{ or } \ln\frac{C_0}{C_t} = \ln\frac{A_0}{A_t} = -k_{app}t,$$

where C_t is the concentration of *p*-NBA at time *t* and k_{app} is the apparent rate constant.

Based on the linear plots of $\ln(C/C_0)$ versus *t*, the values of the apparent rate constant k_{app} at different temperatures were calculated. The apparent constants of *p*-NBA reduction at a temperature interval from 25 to 55 °C are in the range of 0.030 and 0.051 min^{-1}. The activation energy calculated from the Arrhenius equation is equal to 13.80 kJ mol^{-1}. In the course of cyclic hydrogenation of p-NBA, the content of AuNPs is reduced due to either aggregation or leaching out of AuNPs from the cryogel matrix (Fig. 9).

Such a phenomenon was also observed for PVP protected PdNPs immobilized within the gel matrix of polyacrylamide after hydrogenation of the successive portions of allyl alcohol [50]. Moreover, an inward diffusion of metal nanoparticles within the porous structure may also be responsible for deactivation during consecutive catalytic runs.

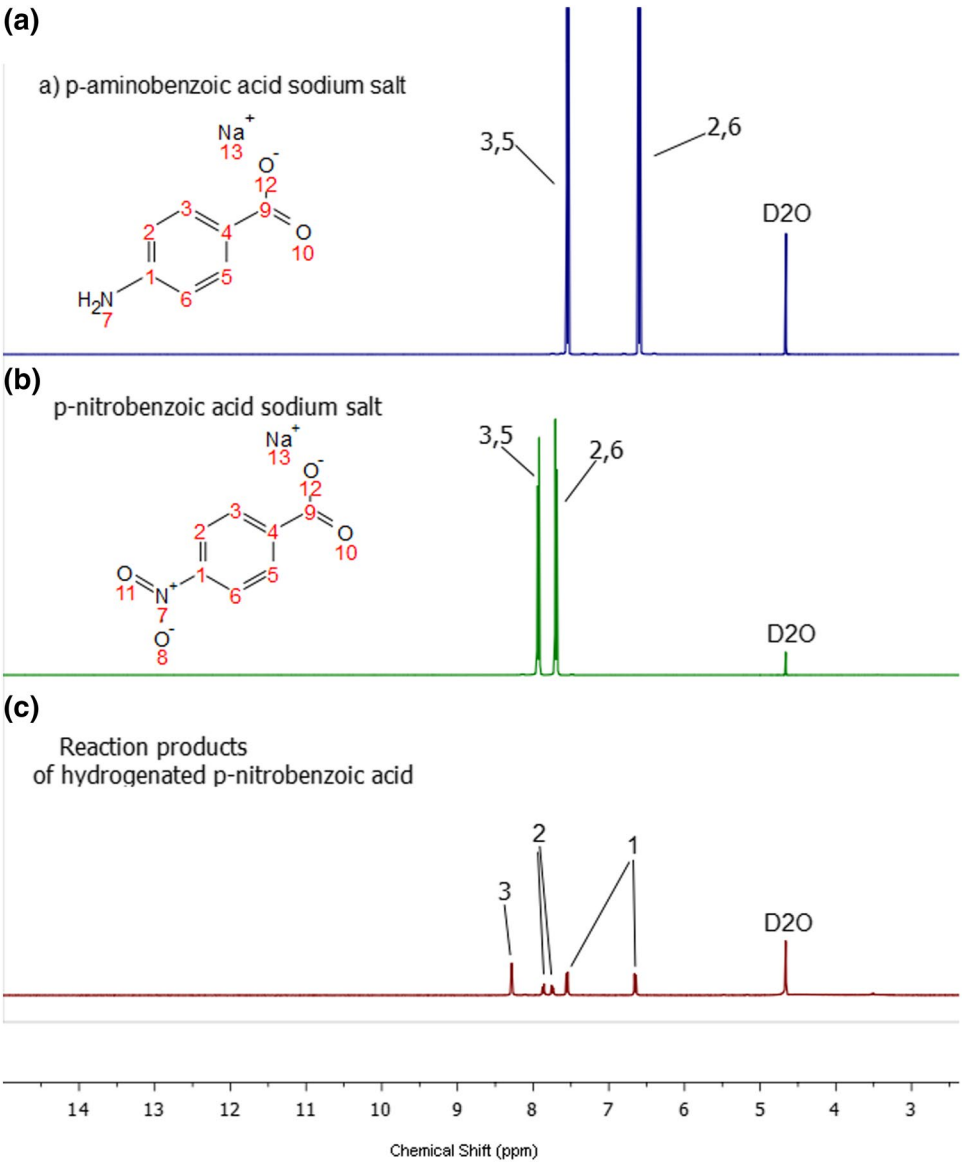

Fig. 6 Comparison of ^{1}H NMR spectra of *p*-ABA (**a**), *p*-NBA (**b**) and hydrogenated product of *p*-NBA (**c**) in D_2O. The signals of reaction products are related to benzene rings of *p*-ABA (1) and *p*-NBA (2), respectively. The signal at δ = 8.28 ppm may be related to NH groups of sodium 4-(4-aminobenzamido) benzoate (3)

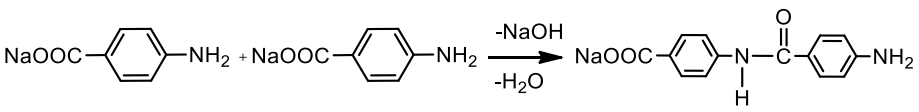

Scheme 3 Proposed mechanism of formation of sodium 4-(4-aminobenzamido)benzoate

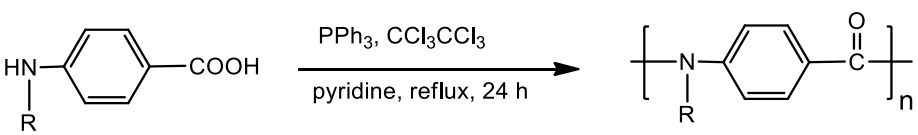

Scheme 4 Condensation polymerization of N-alkylated *p*-aminobenzoic acid. R is H or alkyl groups. Reproduced with permission from Ref. [35]

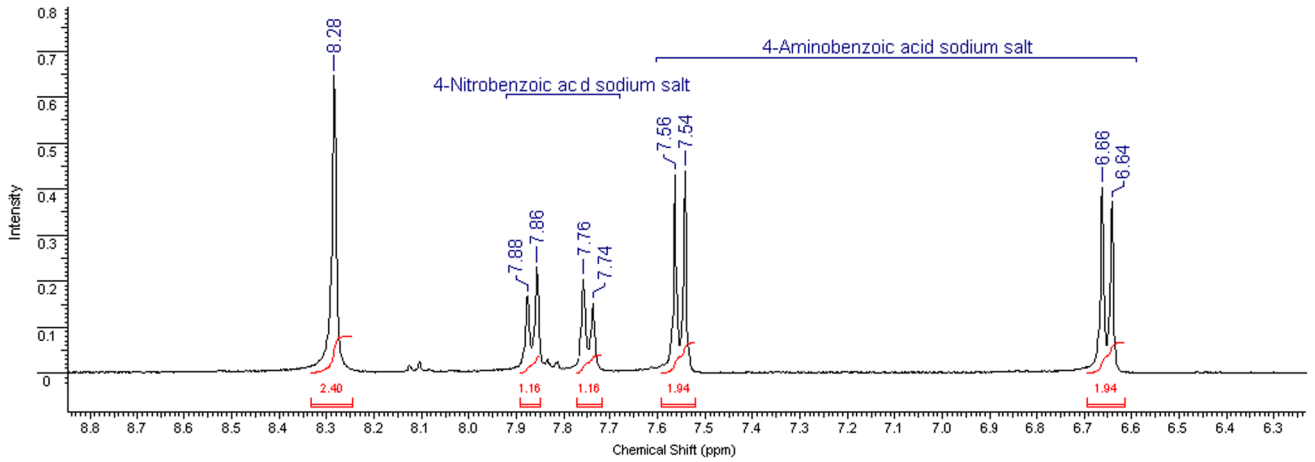

Fig. 7 Scaled ^{1}H NMR spectra of hydrogenated *p*-NBA over DMAEM-*co*-MAA/AuNPs catalyst

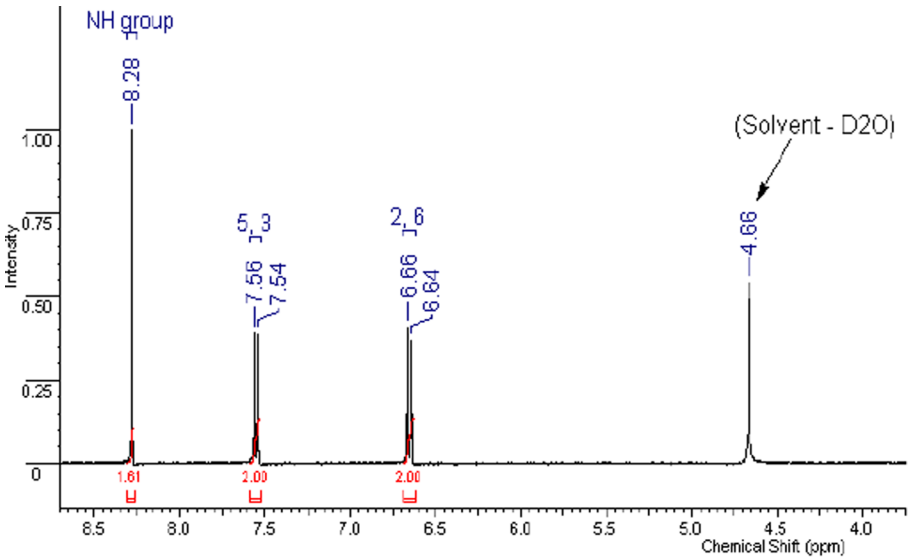

Fig. 8 ^{1}H NMR spectra of pure *p*-ABA passed 5–10 times through DMAEM-*co*-MAA/AuNPs

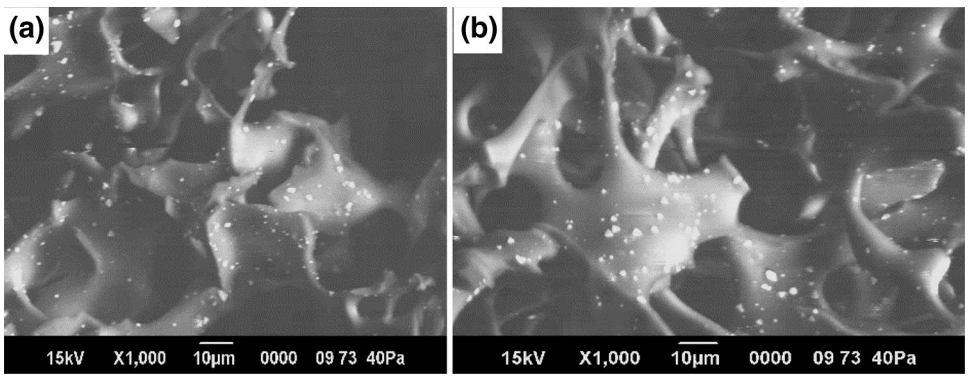

Fig. 9 SEM images of AuNPs on the surface (**a**) and longitudinal (**b**) sections of DMAEM-co-MAA/AuNPs specimen after 10 hydrogenation cycles of p-NBA

3.3 Proposed Mechanism of *p*-NBA Hydrogenation Over DMAEM-*co*-MAA/AuNPs

The proposed mechanism of *p*-NBA reduction is based on literature data [47, 51]. According to a survey of the literature [52], the reduction of *p*-NBA as a heterogeneous catalytic reaction takes place on the surface of AuNPs adsorbed on the surface of cryogel. At first, the *p*-NBA is fixed on the surface of amphoteric cryogel via electrostatic attraction between tertiary amine groups of the cryogel matrix and nitrocarboxyalate ions of *p*-NBA. Three different routes of *p*-NBA conversion are proposed. In all cases the immobilized AuNPs in cryogel pores generates hydrogen atoms from the $NaBH_4$, which in its turn hydrogenate the nitro groups and participate in formation of intermediate nitroso and hydroxylamine compounds.

Utilizing the first route, the AuNPs react with $NaBH_4$ and form the metal hydride on the surface of AuNPs (step 1). In step 2, the formation of nitroso compound is accompanied by elimination of water molecules. In step 3, the nitroso compound is converted to hydroxylamine. In steps 4–6, the hydroxylamine is reduced to an amine (Scheme 5).

With regards to the second route, the condensation of nitroso compound with hydroxylamine produces the azoxy compound (Step i), which is reduced in a series of consecutive steps (Steps ii and iii) to the azo groups (Scheme 6).

The proposed mechanism of formation of *p,p′*-azodibenzoate on DMAEM-*co*-MAA/AuNPs is in good agreement with the reaction route for photoreduction of *p*-NBA on nanostructured silver through photoinduced surface catalytic coupling reactions utilized by other authors [48, 49].

Finally, in the framework of the third route, the aminocarboxylate ions fixed on the surface of the cryogel matrix undergo further conversion to form sodium 4-(4-aminobenzamido)benzoate, as observed in Scheme 7.

Thus, the hydrogenation of *p*-NBA over DMAEM-*co*-MAA/PdNPs produces at least 3 products, including an amino-derivative, azo-derivative and amido-derivative.

3.4 Hydrogenation of *p*-NBA on DMAEM-*co*-MAA/PdNPs

Absorption spectra of *p*-NBA, beginning from a prisitine sample, passed 10 times through the cryogel sample made from DMAEM-*co*-MAA/PdNPs at various molar ratios of substrate to reducing agent are demonstrated in Fig. 10. In this experiment, the flow rate of *p*-NBA through the cryogel sample was equal to 1.5 mL min^{-1}.

The intensity of absorption spectra decreases with decreasing of the molar ratio of substrate to reducing agent. Conversion degree of *p*-NBA to *p*-ABA over

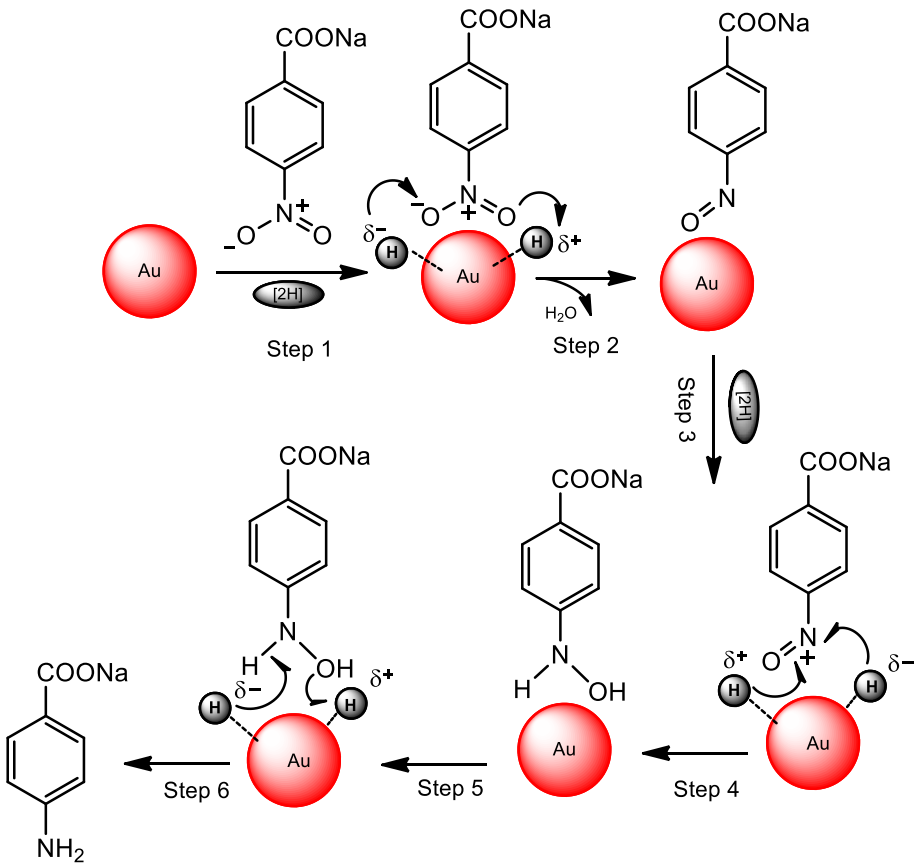

Scheme 5 The proposed mechanism of hydrogenation of *p*-NBA to *p*-ABA

Scheme 6 The proposed mechanism of formation of *p,p′*-azodibenzoate

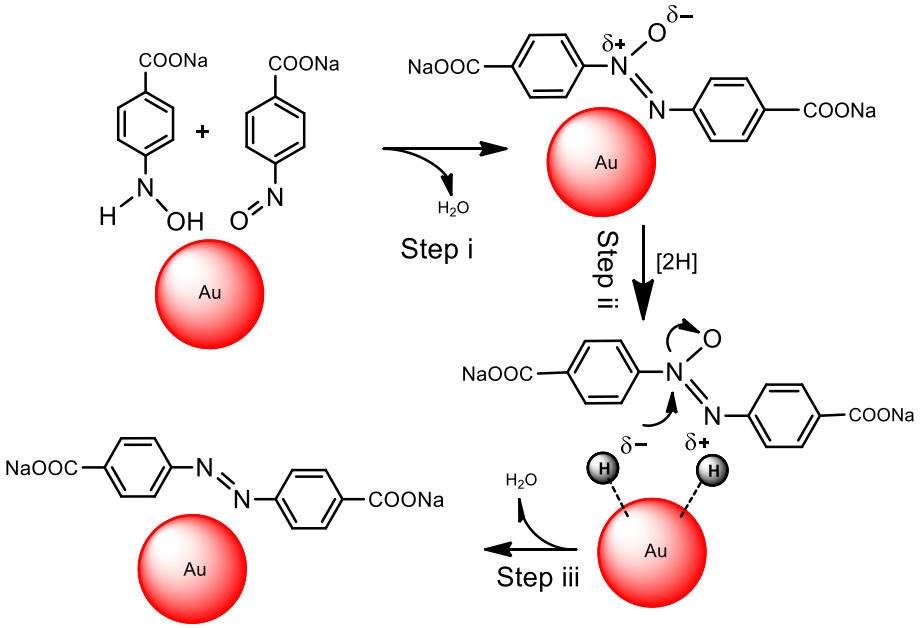

Scheme 7 The proposed mechanism of formation of sodium 4-(4-aminobenzamido) benzoate

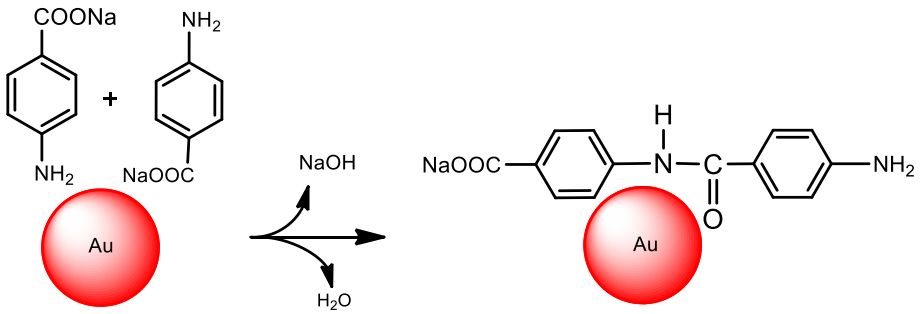

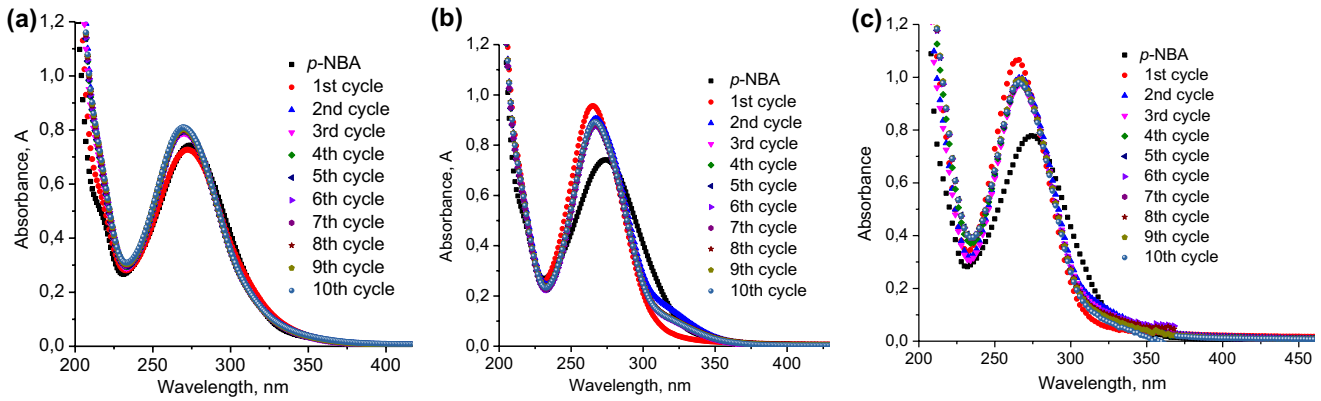

Fig. 10 Absorption spectra of cyclic hydrogenation of *p*-NBA at various molar ratios of substrate to reducing agent. [*p*-NBA]:[$NaBH_4$] = 1:50 (**a**), 1:100 (**b**) and 1:200 (**c**). [*p*-NBA] = 5×10^{-5} mol L^{-1}, T = 298 K

DMAEM-*co*-MAA/PdNPs over 10 cycles and time intervals from 15 to 80 min is shown in Table 2.

As distinct from DMAEM-*co*-MAA/AuNPs catalyst, the formation of by-products is not observed in case of DMAEM-*co*-MAA/PdNPs. As seen in Table 2, approximately 40% of *p*-NBA is converted to *p*-ABA at [PNBA]:[$NaBH_4$] = 1:50 mol/mol, whereas the conversion is full at [PNBA]:[$NaBH_4$] = 1:200 mol/mol. The rate

Table 2 Conversion degree of *p*-NBA to *p*-ABA over DMAEM-*co*-MAA/PdNPs at various molar ratios of substrate to reducing agent

Cycles	Conversion degree, %		
	[PNBA]:[$NaBH_4$] = 1:50 mol/mol	[PNBA]:[$NaBH_4$] = 1:100 mol/mol	[PNBA]:[$NaBH_4$] = 1:200 mol/mol
1	0.95	100	100
2	39.02	89.84	100
3	34.73	82.77	100
4	38.10	78.48	100
5	38.40	78.78	100
6	39.63	78.78	100
7	39.94	80.01	100
8	39.94	84.34	100
9	40.55	84.92	100
10	44.23	84.62	100
Average	39.93[a]	84.28	100

[a]Excepting for the first cycle

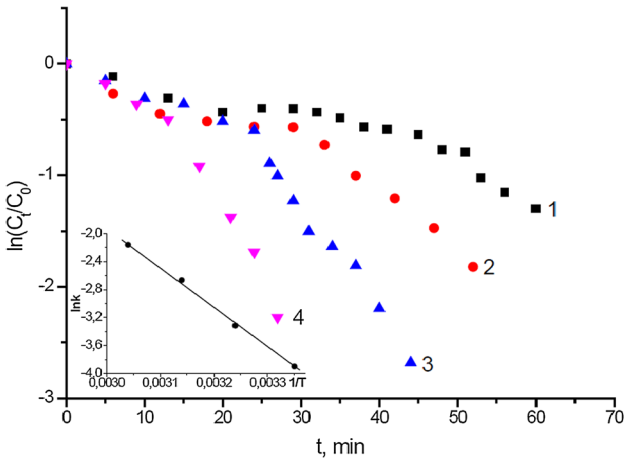

Fig. 11 Kinetic curves of *p*-NBA reduction over DMAEM-*co*-MAA/PdNPs are expressed in the graph $\ln(C_t/C_o)$ versus time. The insert shows lnk versus 1/T. T = 298 (1), 308 (2), 318 (3) and 328 K (4)

constants and activation energy of *p*-NBA reduction over DMAEM-*co*-MAA/PdNPs are represented in Fig. 11. The E_a of *p*-NBA reduction on DMAEM-*co*-MAA/PdNPs is equal to 38.83 kJ mol^{-1}.

Thus, the preparation protocol of amphoteric cryogel based catalyst is very simple, and the catalytic reduction of nitroaromatic compounds with the help of a flow-through catalytic reactor is green and cost-effective, exhibiting a great potential for practical application.

4 Conclusion

The AuNPs and PdNPs were immobilized within the cryogel matrix of DMAEM-*co*-MAA. Both the surface and inner parts of cryogels are mostly covered by AuNPs of different sizes. Passing the mixture of *p*-NBA and $NaBH_4$ through amphoteric cryogel containing AuNPs leads to reduction of *p*-NBA to *p*-ABA and by-products. According to UV–Vis and ^{1}H NMR data, approximately 58–62.6% of *p*-NBA is converted to *p*-ABA with activation energy of 13.80 kJ mol^{-1}. With DMAEM-co-MAA/AuNPs, starting from the 6th cycle of *p*-NBA hydrogenation, an additional two absorption peaks at 285 and 315 nm are observed. The current researchers consider the appearance of the two additional absorption peaks to be connected with formation of *p,p′*-azodibenzoate. Another by-product of *p*-NBA hydrogenation is sodium 4-(4-aminobenzamido)benzoate, due to condensation of amine and carboxylic groups of *p*-ABA molecules. The proposed mechanism of formation of *p,p′*-azodibenzoate and 4-(4-aminobenzamido)benzoate is confirmed by Raman spectroscopy and ^{1}H NMR. Cyclic reduction of sequental portions of *p*-NBA decreases the amount of AuNPs, due to gold nanoparticles partly leaching out from the cryogel surface in comparison with the initial state. Hydrogenation of *p*-NBA by DMAEM-*co*-MAA/PdNPs proceeds without formation of by-products and yields only *p*-ABA with activation energy of 38.83 kJ mol^{-1}. Due to the dependence of the molar ratio of substrate to reducing agent, the conversion degree of *p*-NBA to *p*-ABA varies from 40 to 100%. The potential application of amphoteric cryogel samples with immobilized AuNPs and PdNPs as effective flow-through units for continuous hydrogenation of *p*-NBA has been demonstrated, and the results obtained may provide a new strategy for the syntheses of amino compounds, azo dyes, or benzamides from aromatic nitro compounds on palladium and gold nanoparticles immobilized within a cryogel matrix.

Acknowledgements Financial support from the Ministry of Education and Science of the Republic of Kazakhstan (IRN AP05131003, 2018–2020) is greatly acknowledged.

Compliance with Ethical Standards

Conflict of interest The authors declare that they have no conflict of interest.

References

1. E.A. Bekturov, S.E. Kudaibergenov, *Catalysis by Polymers* (Wiley, New York, 2008)
2. A.D. Pomogailo, G.I. Dzhardimalieva, *Metallopolymeric Hybrid Nanocomposites* (Nauka, Moscow, 2015)
3. Zh.E. Ibrayeva, S.E. Kudaibergenov, E.A. Bekturov, *Stabilization of Metal Nanoparticles by Hydrophilic Polymers (in Russian)* (LAP Lambert Academic Publishing, Germany, 2013)
4. G.I. Dzhardimalieva, V.G. Dorokhov, N.D. Golubeva, S.I. Pomogailo, A.M. Lyakhovich, V.I. Savchenko, A.D. Pomogailo, Russ. Chem. Bull. Int. Ed. 58, 2070 (2009)
5. S.E. Kudaibergenov, G.S. Tatykhanova, B.S. Selenova, J. Inorg. Organomet. Polym. **26**, 1198 (2016)
6. S.E. Kudaibergenov, N. Nuraje, V.V. Khutoryanskiy, Soft Matter **8**, 9302 (2012)
7. V.I. Lozinsky, Russ. Chem. Rev. **71**, 489 (2002)
8. V.I. Lozinskiy, I.Y. Galaev, F.M. Plieva, I.N. Savina, H. Jungvid, B. Mattiasson, Trends Biotechnol. **10**, 445 (2003)
9. V.I. Lozinsky, Adv. Polym. Sci. **263**, 1 (2014)
10. F. Hapiot, S. Menuel, E. Monflier, ACS Catal. **3**, 1006 (2013)
11. C. Yang, G.-F. Liu, X.-L. Zhou et al., Catal. Lett. **145**, 1778 (2015)
12. N. Sahiner, S. Yildiz, M. Sahiner, Z.A. Issa, H. Al-Lohedan, Appl. Surf. Sci. **354**, 388 (2015)
13. N. Sahiner, F. Seven, Energy **71**, 170 (2014)
14. N. Sahiner, S. Yildiz, Fuel Process. Technol. **126**, 324 (2014)
15. N. Sahiner, F. Seven, RSC Adv. **4**, 23886 (2014)
16. M. Ajmal, M. Siddiq, N. Aktas, N. Sahiner, RSC Adv. **5**, 43873 (2015)
17. B. Andersson, AlChE J. **28**, 333 (1982)
18. E.F. Litvin, L.K. Freidlin, R.N. Gurskii, R.V. Istratova, I.L. Vaisman, Bull. Acad. Sci. USSR Chem. Sci. **24**, 1620 (1975)
19. P.A. Simonov, A.V. Romanenko, V.A. Likholobov, Solid Fuel Chem. **48**, 364 (2014)
20. S. Jana, S. Pande, A.K. Sinha, S. Sarkar, M. Pradhan, M. Basu, Y. Negishi, A. Pal, T. Pal, Langmuir **10**, 847 (2010)
21. G.N. Al'tshuler, G.Yu. Shkurenko, A.A. Gorlov, Russ. J. Phys. Chem. A **89**, 372 (2015)
22. S. Jana, S. Pande, S. Panigrahi, S. Praharaj, S. Basu, A. Pal, T. Pal, Langmuir **22**, 7091 (2006)
23. W. Wang, Y. Song, Q. Lin, K. Yang, Bull. Mater. Sci. **37**, 797 (2014)
24. C. Fernandez, E. Lujano, U. Macias, et al., Catal. Lett. **95**, 143 (2004)
25. F. Lapicque, A. Storck, J. Appl. Electrochem. **16**, 825 (1986)
26. M.G. Abdullaev, Z.Sh. Abdullaeva, M.V. Klyuev, Z.G. Gebekova, Pharm. Chem. J. **48**, 343 (2014)
27. H.-G. Zendel, M. Bergfeld, USSR Patent No. 511851. Published 25.04.76 in Bulletin of Invention No. 15
28. K. Amei, H. Eshghi, M. Bakavol, S. Rostamnia, Catal. Lett. **147**, 491 (2016)
29. N. Mei, B. Liu, Int. J. Hydrog. Energy (2016). https://doi.org/10.1016/j.ijhydenc.2016.07.229
30. R.M. Magdalene, E.G. Leelamani, N.M.N. Gowda, J. Mol. Catal. A **223**, 17 (2004)
31. M. Tian, C. Dong, Z. Dong, Appl. Surf. Sci. **390**, 100 (2016)
32. P. Zhou, D. Li, S. Jin, S. Chen, Z. Zhang, Int. J. Hydrog. Energy (2016). https://doi.org/10.1016/j.ijhydenc.2016.07.257
33. P.F. Vogt, J.J. Gerulis, *Amines, Aromatic. Ullmann's Encyclopedia of Industrial Chemistry* (Wiley, New York, 2000)
34. S.E. Kudaibergenov, G.S. Tatykhanova, A.N. Klivenko, J. Appl. Polym. Sci. (2016). https://doi.org/10.1002/app.43784
35. A.N. Klivenko, G.S. Tatykhanova, N. Nuraje, S. Kudaibergenov, Bull. Karaganda Univ. Ser. Chem. **4**(80), 10 (2015)
36. G.S. Tatykhanova, A.N. Klivenko, G.M. Kudaibergenova, S.E. Kudaibergenov, Macromol. Symp. **363**, 49 (2016)
37. M. Aldabergenov, M Dauletbekova, A. Shakhvorostov, G. Toleutay, A. Klivenko, S. Kudaibergenov, J. Chem. Technol. Metall. **53**, 11 (2018)
38. A. Gainar, J.S. Stevens, E. Suljoti, J. Xiao, R. Golnak, E.F. Aziz, S.L.M. Schroeder, J. Phys. Conf. Ser. **712**, 012034 (2016)
39. M. Muniz-Miranda, J. Anal. Bioanal. Tech. **6**, 1 (2015)
40. P.G. Roth, R.S. Venkatachalam, F.J. Boerio, J. Chem. Phys. **85**, 1150 (1986)
41. R.S. Venkatachalam, F.J. Boerio, P.G. Roth, J. Raman Spectrosc. **19**, 281 (1988)
42. E.J. Liang, C. Engert, W. Kiefer, Vib. Spectrosc. **6**, 79 (1993)
43. X.M. Yang, D.A. Tryk, K. Hashimoto, A. Fujishima, J. Phys. Chem. B **102**, 4933 (1998)
44. X. Lili, F. Yan, Spectrochim. Acta A **61**, 1991 (2005)
45. H. Park, S.B. Lee, K. Kim, M.S. Kim, J. Phys. Chem. **94**, 7516 (1990)
46. J.W. Wang, W.N. Wang, Y. Fang, Vib. Spectrosc. **40**, 197 (2006)
47. L.-B. Zhao, Y.-F. Huang, X.-M. Liu, J.R. Anema, D.-Y. Wu, B. Ren, Z.-Q. Tian, Phys. Chem. Chem. Phys. **14**, 12919 (2012)
48. V.R.P. Verneker, B. Shahat, Macromolecules **19**, 1851–1856 (1986)
49. Y. Shibasaki, Y. Abe, N. Sato, A. Fujimori, Y. Oishi, Polym. J. **42**, 72 (2010)
50. S.E. Kudaibergenov Zh.E. Ibraeva, N.A. Dolya, B.Kh. Musabayeva, A.K. Zharmagambetova, J. Koetz. Macromol. Symp. **274**, 11 (2008)
51. P. Veerakumar, M. Velayudham, K.-L. Lu, S. Rajagopal, Appl. Catal. A **439**, 197 (2012)
52. D. Wu, Y. Zhang, M. Wen, H. Fang, Q. Wu, Inorg. Chem. (2017). https://doi.org/10.1021/acs.inorgchem.7b00304